Timelike geodesic motions within the general relativistic gravitational field of the rigidly rotating disk of dust

M. Ansorg[a)]
Friedrich-Schiller-Universität Jena, Theoretisch-Physikalisches Institut, Max-Wien-Platz 1, D-07743 Jena, Germany

(Received 15 June 1998; accepted for publication 3 August 1998)

The general relativistic motion of a test particle near a rigidly rotating disk of dust is investigated. Circular orbits within the plane of the disk (centered on the rotation axis) are special cases of the geodesic motion. One finds that there is always a (stable or unstable) circular orbit for positive angular momentum and a given radius. However, for sufficiently relativistic disks there are regions within the plane of the disk in which a particle with negative angular momentum cannot follow a circular path. If the disk is still more strongly relativistic, then one finds circular orbits with negative energies of arbitrary magnitude. Within the theoretical construction of the Penrose effect, this property can be used to produce arbitrarily high amounts of energy. The study of Hamiltonian mechanics forms another topic of this article. It turns out that the stochastic behavior of the geodesics is related to the position of the region containing all the crossing points of the particle through the plane of the disk. If this region contains points lying inside the disk as well as points outside, the geodesic motion shows highly stochastic behavior. However, if the crossing region is completely inside or outside the disk, the motion proves to be nearly integrable. In these cases the corresponding Hamiltonian system is close to an integrable system of the so-called Liouville class. [S0022-2488(98)03711-6]

I. INTRODUCTION

Einstein's general theory of relativity describes gravitation as a geometric property of the four-dimensional manifold of space and time. Particles moving merely under the influence of gravitation follow the so-called timelike geodesic paths. The investigation of these curves helps in the understanding of the geometrical structure of the manifold in question. Furthermore, accretion processes in which matter is drawn into a central object (e.g., a black hole or a disklike formation) may be approximated by the assumption that the inflowing matter follows the timelike geodesics.

The famous Kerr black hole was the first rotating object for which the relativistic field equations were solved. The timelike geodesic motions near a Kerr black hole have been studied in detail (see, e.g., Ref. 1). For them the corresponding Hamiltonian–Jacobi equation is separable,[2] and the equations of motions are integrable by quadratures. As a consequence, in phase space the trajectories lie within surfaces diffeomorphic to tori.

The general relativistic gravitational field created by a rigidly rotating disk of dust was first studied numerically in 1971 by Bardeen and Wagoner.[3] The global analytic solution of Einstein's field equations for this object was found in 1995 by Neugebauer and Meinel.[4] Their explicit expressions for the metric coefficients allow a direct numerical implementation of the geodesic equations.

In this paper the bounded motions around a rigidly rotating disk of dust are investigated. It turned out that these motions are not integrable by quadratures. In phase space they occupy regions of more complicated structure. However, for a considerable fraction of the set of all bounded timelike geodesic motions, particular properties can be found.

[a)]Electronic mail: Ansorg@hpfs1.tpi.uni-jena.de

A. The metric

Einstein's field equations for a rigidly rotating disk of dust can be reduced to a single nonlinear complex partial differential equation—the so-called Ernst equation—for which a boundary value problem has to be solved.[5,6] Neugebauer and Meinel succeeded in solving this problem by means of the inverse scattering method which is a technique from the soliton theory.

Writing the metric in Weyl–Papapetrou coordinates (ρ,ζ,φ,t) in the form (a comma in an index represents a partial derivative, a semicolon stands for a covariant derivative)

$$(g_{ij})=\begin{pmatrix} e^{2(k-U)} & 0 & 0 & 0 \\ 0 & e^{2(k-U)} & 0 & 0 \\ 0 & 0 & -a^2e^{2U}+\rho^2e^{-2U} & -ae^{2U} \\ 0 & 0 & -ae^{2U} & -e^{2U} \end{pmatrix} \quad \text{with} \quad g_{ij,\varphi}=0=g_{ij,t},$$

the field equations turn out to be equivalent to the Ernst equation

$$\Re f\left(f_{,\rho\rho}+f_{,\zeta\zeta}+\frac{f_{,\rho}}{\rho}\right)=f_{,\rho}^2+f_{,\zeta}^2$$

for the Ernst potential f which is defined by

$$f=e^{2U}+ib \quad \text{with} \quad b_{,\zeta}=\frac{e^{4U}}{\rho}\,a_{,\rho}, \quad b_{,\rho}=-\frac{e^{4U}}{\rho}\,a_{,\zeta}.$$

The remaining metric function k can be calculated from the functions U and a by quadratures.

Neugebauer and Meinel found the Ernst potential for the rigidly rotating disk of dust in terms of ultraelliptic functions.[4] In their expressions, the Ernst potential depends on a parameter μ, which is related to the angular velocity Ω and the radius ρ_0 of the disk by

$$\mu=2\Omega^2\rho_0^2e^{-2V_0} \quad \text{with} \quad V_0(\mu)=U(\rho=0,\zeta=0;\mu).$$

The parameter μ lies within the interval $(0,\mu_0)$ with $\mu_0=4.629\,66...$. For $\mu\ll1$, one obtains the Newtonian limit of the Maclaurin disk; $\mu\to\mu_0$ and $\rho_0\to0$ yield the extreme Kerr solution. The disk creates an ergosphere [i.e., a region within which the metric function $(-e^{2U})$ is positive] for $\mu>\mu_e\approx1.69$.

In what follows, units are used where the radius ρ_0 as well as the velocity of light c are equal to 1.

B. The Hamiltonian system of the geodesic equations

For axisymmetric stationary space–times the general Hamiltonian system

$$\mathscr{H}=\frac{1}{2}\,g^{ij}p_ip_j \quad \text{with} \quad p_i=g_{ij}\dot{x}^i, \quad \left(=\frac{d}{d\tau}, \quad \tau\text{:proper time}\right)$$

for the timelike geodesic equations

$$\ddot{x}^i+\Gamma^i_{kl}\dot{x}^k\dot{x}^l=0, \quad \dot{x}_k\dot{x}^k=-1$$

can be reduced to a conservative Hamiltonian of two degrees of freedom of the following form:

$$\mathscr{H}=\frac{1}{2}\,e^{2(U-k)}(p_\rho^2+p_\zeta^2)+\frac{1}{2}\left[1-\frac{1}{\rho^2}\,(L^2g_{tt}+2LEg_{\varphi t}+E^2g_{\varphi\varphi})\right]. \tag{1}$$

Here, $L=p_\varphi=\text{const}$ is called the (ζ component of the) angular momentum of the particle and $E=-p_t=\text{const}$ its energy.

The above Hamiltonian is invariant under a simultaneous change of the signs of L and E. Now, these signs are fixed by the condition $\dot{t}>0$ and this condition is then satisfied along the whole trajectory.

The Hamiltonian (1) is arranged such that $\mathscr{H}=0$ holds along the trajectory of the considered test particle. Therefore a restricting condition for the region in which the motion takes place is given by

$$0\leqslant e^{2(U-k)}(p_\rho^2+p_\zeta^2)=\left[\frac{1}{\rho^2}\,(L^2 g_{tt}+2LEg_{\varphi t}+E^2 g_{\varphi\varphi})-1\right]. \tag{2}$$

This region of motion has the following properties:

(1) The region is bounded for $E^2<1$. For $E^2\geqslant 1$ there are unbounded areas allowing an escape of the test particle to infinity. But also, in the case of $E^2\geqslant 1$, there may be additional bounded regions which force the particle to stay inside.
(2) Particles with $L\neq 0$ may not cross the rotation axis.
(3) The momenta p_ρ and p_ζ as well as the velocities $\dot{\rho}$ and $\dot{\zeta}$ vanish at the rim of the considered region. Furthermore, at the boundary of the region the acceleration vector $(\ddot{\rho},\ddot{\zeta})$ is perpendicular to the curve of the boundary and points inwards.
(4) Because of the property $g_{ij}(\rho,-\zeta)=g_{ij}(\rho,\zeta)$, the regions of motion are symmetric with respect to reflection in the plane of the disk.

Illustrative examples for bounded regions of motion can be seen in Figs. 9, 10, 18, and 20.

II. CIRCULAR ORBITS

Motions within the plane of the disk are described by a Hamiltonian with merely one degree of freedom. By the conditions $\dot{\rho}=0=\ddot{\rho}$, circular orbits with centers on the rotation axis are fixed. The following numerical results about circular orbits contain in particular Meinel's and Kleinwächter's analytic results about circular orbits at the rim of the disk.[7] The above conditions $\dot{\rho}=0=\ddot{\rho}$ lead to the equations

$$\begin{aligned} L^2 g_{tt}(\rho,0)+2LEg_{\varphi t}(\rho,0)+E^2 g_{\varphi\varphi}(\rho,0)&=\rho^2,\\ L^2 g_{tt,\rho}(\rho,0)+2LEg_{\varphi t,\rho}(\rho,0)+E^2 g_{\varphi\varphi,\rho}(\rho,0)&=2\rho, \end{aligned} \tag{3}$$

which serve to determine the parameter functions $L_\pm=L_\pm(\rho)$ and $E_\pm=E_\pm(\rho)$. These functions yield for a circular orbit of given radius ρ, the associated pairs of angular momentum and energy. In general, there are two such pairs, denoted by $(L_+(\rho),E_+(\rho))$ and $(L_-(\rho),E_-(\rho))$ where (L_+,E_+) refers to an orbit of positive angular momentum and similarly (L_-,E_-) to an orbit with negative angular momentum. It turns out that the functions $L_+(\rho)$ and $E_+(\rho)$ exist for arbitrary choice of $\rho\geqslant 0$. However, for sufficiently large values of the parameter μ there are no corresponding (L_-,E_-) pairs for ρ values within a certain interval $(\tilde{\rho}_1,\tilde{\rho}_2)$.

In Figs. 1–5, the functions $L_\pm=L_\pm(\rho)$ and $E_\pm=E_\pm(\rho)$ can be seen for different values of the parameter μ. A discussion of these pictures follows.

(1) The pictures for (L_+,E_+) are similar for all values of μ (see Fig. 1). There is a monotonous growth of the functions L_+ and E_+ for $\rho<1$. At $\rho=1$ (here $E_+=1$) both functions turn back and decrease monotonously until they reach another turning point at $\rho=\rho'$. For still greater values of the parameter ρ, the functions L_+ and E_+ grow monotonously again. The turning points are characterized by the conditions $dL_+/d\rho=0=dE_+/d\rho$. As the radius $\rho\to\infty$, E_+ tends to 1 and L_+ to $+\infty$.

Circular orbits with a radius $\rho\in(1,\rho')$ are unstable. Stable circular orbits are those with a radius $\rho\in[0,1)$ or $\rho\in(\rho',\infty)$; the remaining circular orbits with radius 1 or ρ' are marginally unstable.

For circular orbits, the condition

$$\dot{\varphi}=\frac{dE}{dL}\,\dot{t} \tag{4}$$

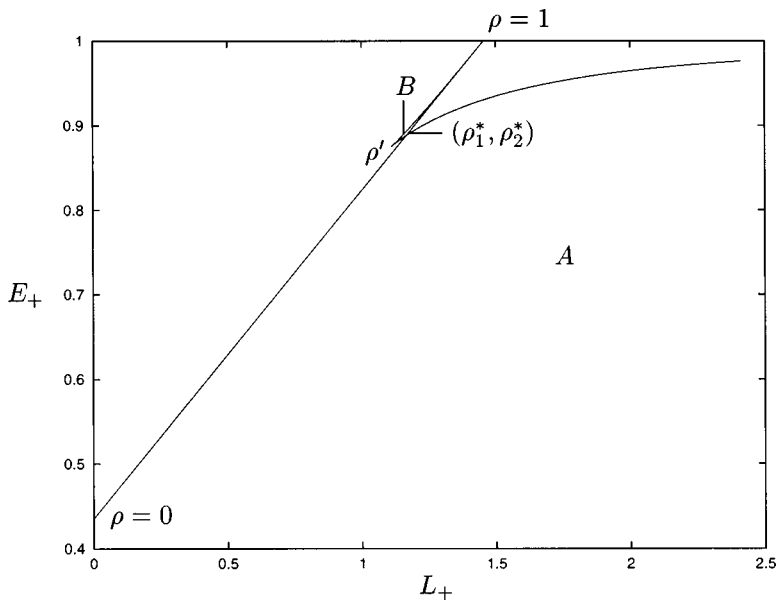

FIG. 1. The functions $L_+(\rho)$ and $E_+(\rho)$ for $\mu = 1.61$.

holds. In all sections of the graphs of the functions L_+ and E_+, the function $E_+ = E_+(L_+)$ grows monotonously. Hence, all circular orbits with positive angular momenta possess positive angular velocity. Furthermore, circular orbits with radii $\rho < 1$ are just those paths along which the dust particles of the disk move. Their four velocity (u^i) is given by $(u^i) = (0,0,\dot{\varphi},\dot{t}) = e^{-V_0}(0,0,\Omega,1)$ (see Ref. 8) from which $dE/dL = \Omega = \text{const}$ follows. Thus, the graph $E_+(L_+)$ is a straight line for $\rho \in [0,1]$.

The region A contains all (L,E) pairs for which no motion of a particle is possible, i.e., either the restricting condition (2) cannot be satisfied or the motion possesses a negative $\dot{t}$. If one chooses for a (not necessarily circular) motion, an (L,E) pair inside the small region B, then there exist two separate compact regions in which bounded motions are possible. At the intersection point of the stable and unstable parts of the (L_+, E_+) graphs these regions degenerate into two

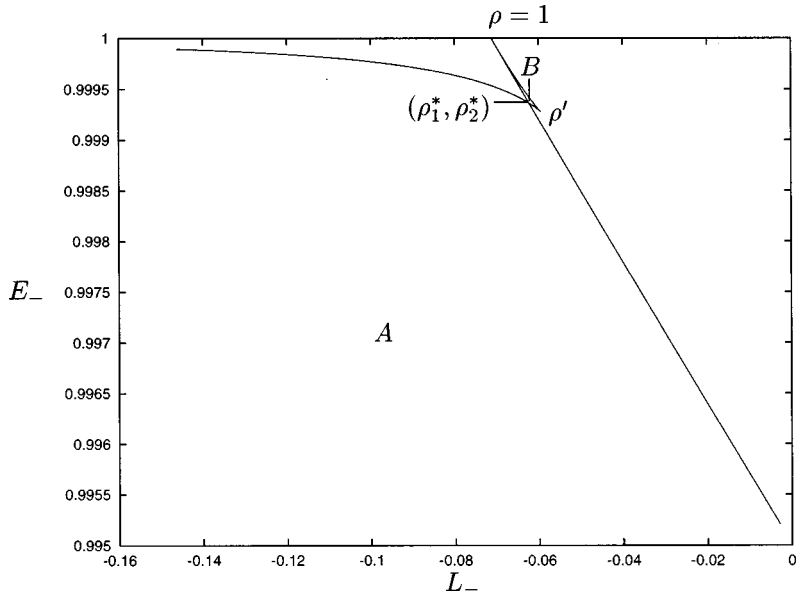

FIG. 2. The functions $L_-(\rho)$ and $E_-(\rho)$ for $\mu = 0.01$.

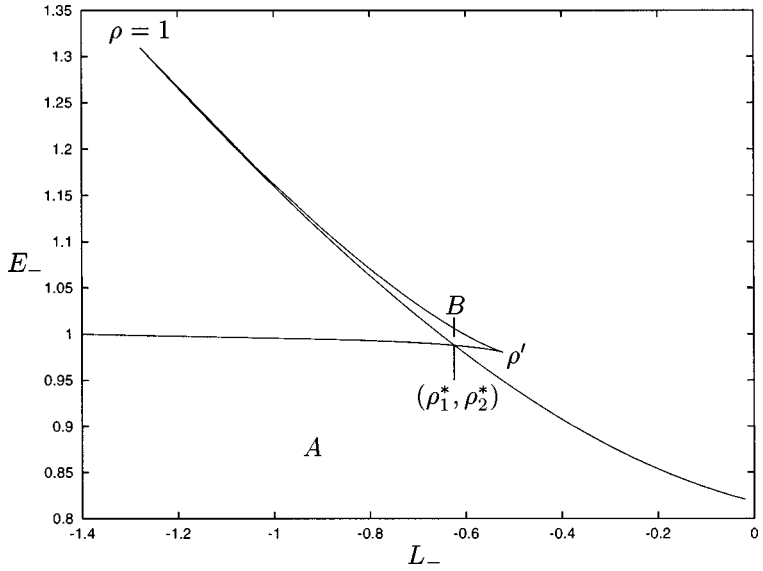

FIG. 3. The functions $L_-(\rho)$ and $E_-(\rho)$ for $\mu = 0.4$.

separate stable circular orbits with radii $\rho_1^* < 1$ and $\rho_2^* > 1$. In Fig. 6, it can be seen how the radii ρ_1^*, ρ_2^*, and ρ' depend on the parameter μ.

(2) In Figs. 2–5, the parameter functions $L_-(\rho)$ and $E_-(\rho)$ are displayed for different values of the parameter μ. For $0 < \mu < 1/2$, the pictures are similar to the graphs of the functions L_+ and E_+. The region B extends now to E_--values greater than 1. Thus, there are stable as well as unstable circular orbits, and furthermore, extended compact regions of motions with energies greater than 1 and corresponding negative angular momenta. From Eq. (4) and the slopes of the functions $E_- = E_-(L_-)$ in Figs. 2 and 3, one concludes that all particles moving along circular orbits with negative angular momenta have negative angular velocity.

(3) As μ approaches the value $\frac{1}{2}$, the region B grows and is unbounded for $\mu \geqslant 1/2$. For radii $\rho \in (\tilde{\rho}_1, \tilde{\rho}_2)$ there are no circular orbits with negative angular momentum. As can be seen in Fig. 4, for sufficiently large values of μ ($\mu > \mu_{\dot{\varphi}} \approx 0.7088$) there are small intervals $[0, \rho_{\dot{\varphi}})$ in which the functions $E_-(L_-)$ grow monotonously. Hence, circular orbits with radii $\rho < \rho_{\dot{\varphi}}$ possess positive

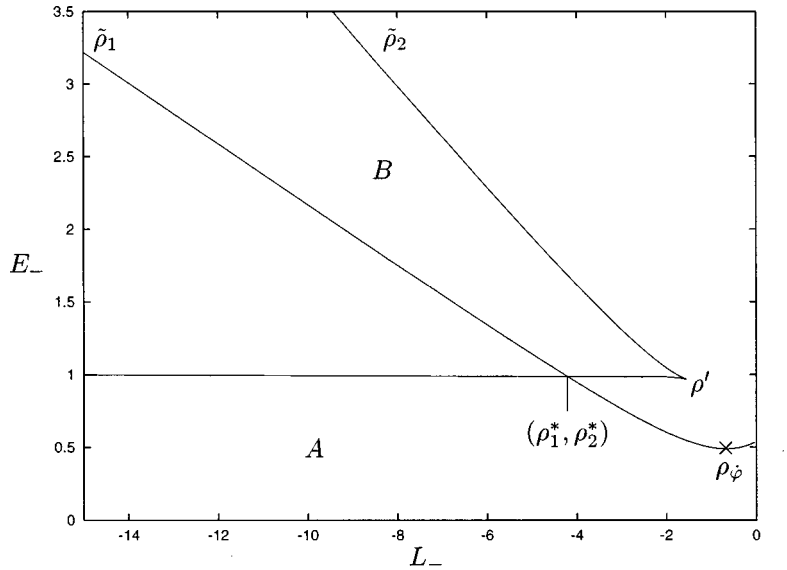

FIG. 4. The functions $L_-(\rho)$ and $E_-(\rho)$ for $\mu = 1.21$.

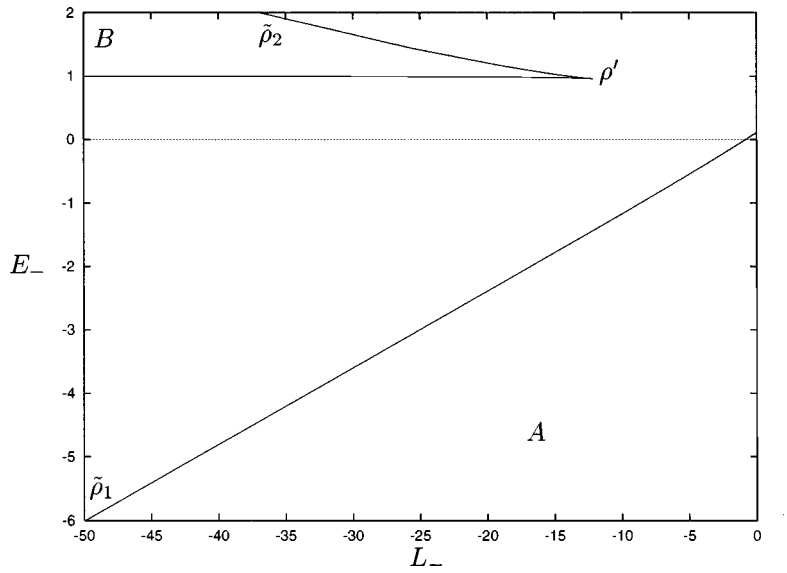

FIG. 5. The functions $L_-(\rho)$ and $E_-(\rho)$ for $\mu=3.5$.

angular velocities in spite of having negative angular momenta. At the radius $\rho_{\dot{\varphi}}$ a particle may remain at rest (in the chosen coordinate system). Such a particle has the smallest energy possible of all motions around the disk.

(4) Finally, in the range $\mu_e<\mu<\mu_0$ (see Fig. 5), there are stable circular orbits with negative energies. As the slope of $E_-(L_-)$ is positive for $\rho<\tilde{\rho}_1$, circular orbits with radii in this range have positive angular velocities. The μ dependencies of the radii $\{\rho_1^*,\rho_2^*,\rho',\tilde{\rho}_1,\tilde{\rho}_2,\rho_{\dot{\varphi}}\}$ as well as those of the radii $\rho_1^{(E)}$ and $\rho_2^{(E)}$, at which the function $E_-=E_-(\rho)$ reaches the value $E_-(\rho_i^{(E)})=1$, are displayed in Fig. 7.

(5) As $\mu\to 0$, the curves $L_\pm(\rho)$ and $E_\pm(\rho)$ tend to the corresponding graphs for the Maclaurin disk (the Newtonian limit of the relativistic disk). Since negative and positive angular momenta are equivalent in Newtonian theory, these graphs possess a reflectional symmetry with respect to the axis $L=0$.

Circular orbits around a Kerr black hole are characterized by the functions (see, e.g., Ref. 1)

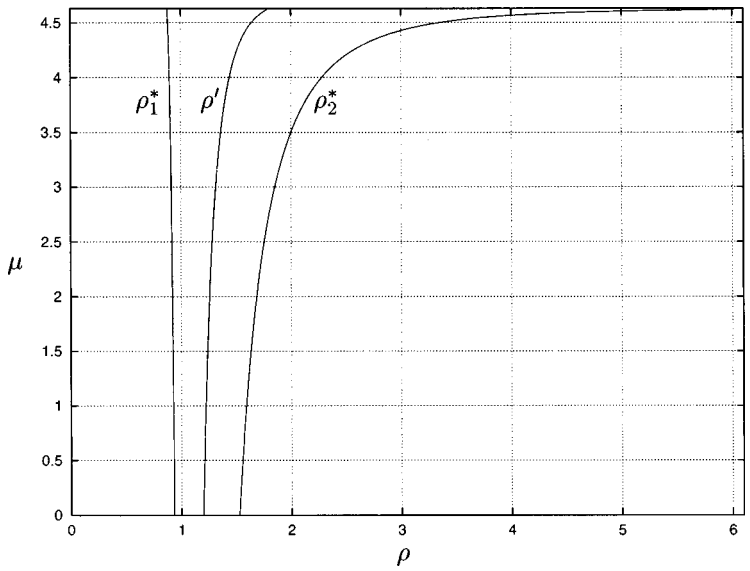

FIG. 6. The μ dependency of the radii ρ_1^*, ρ_2^*, and ρ' for the functions L_+ and E_+.

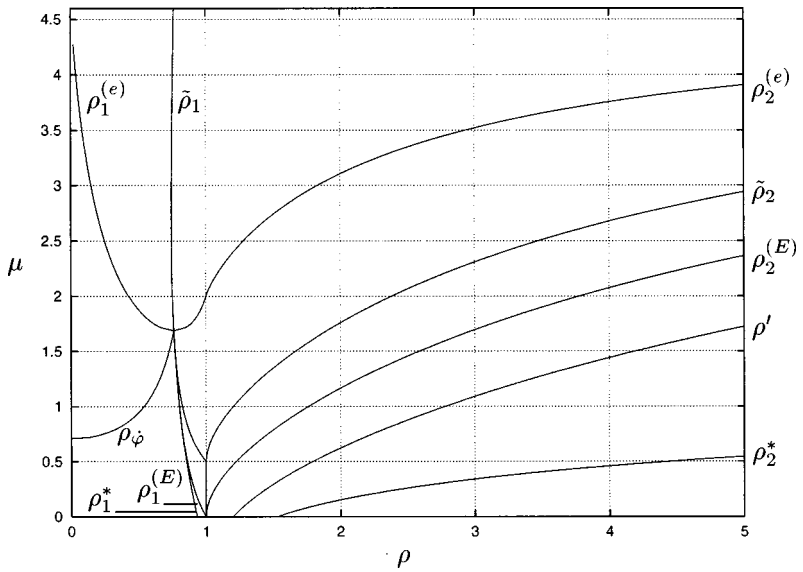

FIG. 7. The μ dependency of the radii $\{\rho_1^*,\rho_2^*,\rho',\tilde{\rho}_1,\tilde{\rho}_2,\rho_{\dot{\varphi}},\rho_1^{(E)},\rho_2^{(E)}\}$ for the functions L_- and E_-. Additionally, the radii $\rho_1^{(e)}$ and $\rho_2^{(e)}$, at which the ergosphere intersects the plane of the disk, are plotted.

$$E_\pm=\frac{r^{3/2}-2mr^{1/2}\pm am^{1/2}}{r^{3/4}(r^{3/2}-3mr^{1/2}\pm 2am^{1/2})^{1/2}},\quad L_\pm=\pm\frac{m^{1/2}[r^2\mp 2a(mr)^{1/2}+a^2]}{r^{3/4}(r^{3/2}-3mr^{1/2}\pm 2am^{1/2})^{1/2}},$$

where $\rho=\sqrt{r^2-2mr+a^2}$, m denotes the mass, and a the specific angular momentum of the black hole. For vanishing denominator in the above expressions (this may happen as ρ reaches the value $\tilde{\rho}$), $L_\pm\to\pm\infty$ and $E_\pm\to+\infty$. Circular orbits with radii less than $\tilde{\rho}$ do not exist. For $\rho>\tilde{\rho}$, the $(L_\pm,E_\pm)$ curves are similar to those of Fig. 5 for $\rho>\tilde{\rho}_2$. Again there is a ρ' which separates unstable (for $\rho<\rho'$) and stable orbits (for $\rho>\rho'$). Furthermore, for circular orbits within the Kerr metric, the signs of angular momentum and velocity always coincide.

Generally one finds that the qualitative behavior of circular motions at sufficiently large radii is similar for the Kerr black hole and the disk. However, circular motions at small radii are quite different.

III. THE PENROSE EFFECT

The Penrose effect is a theoretical construction to produce energy. A test particle (with angular momentum L_0 and energy E_0) is allowed to fall from infinity (hence $E_0>1$) into the ergosphere of the disk. There, it splits into two particles with angular momenta L_1,L_2 and energies E_1,E_2. The total angular momentum and energy are preserved, i.e.,

$$L_0=L_1+L_2,\quad E_0+E_1+E_2.$$

If one of the created particles possesses negative energy (say $E_1<0$), then the other one has an energy $E_2>E_0$. The latter particle escapes to infinity where its higher energy can be utilized.

If a large amount of energy were to be drawn from the disk by this method, the particles remaining within the ergosphere would have a considerable repercussion on the disk. Hence, in the following considerations, when one speaks about arbitrarily high energies, one still means that these energies are negligible compared to the energy of the disk.

A simple way to produce energy would seem to be the following. A particle with an energy E_0 which is slightly larger than 1 falls from infinity into the ergosphere to the point $(\tilde{\rho}_1,0)$ (see Figs. 5 and 7), where it separates into two particles. After the separation, one of the created particles follows the stable circular orbit at $\tilde{\rho}_1$ and has the energy $E_1=E_-(\tilde{\rho}_1)=-\infty$. Hence, the escaping particle possesses an energy $E_2=\infty$. But this does not work since the outgoing particle cannot satisfy the condition (2) at $(\tilde{\rho}_1,0)$, i.e., it never reaches this point. However, it turns out that

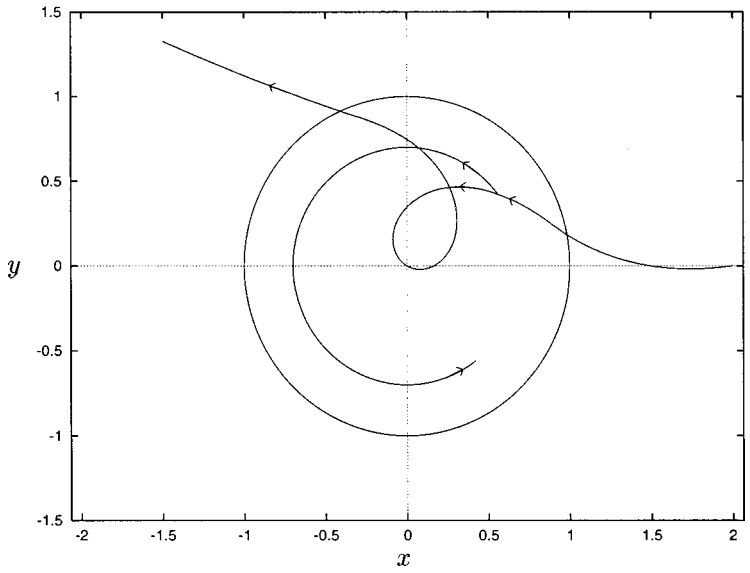

FIG. 8. The Penrose effect. At a value $\mu=2.2$, the parameters $E_0=1.1$ and $\rho_C=0.7$ have been chosen. The energy of the escaping particle is 0.16 greater than the energy of the infalling particle. The curves of the particles can be seen, as the particles move within the plane of the disk (the disk is represented by a circle).

an arbitrary profit of energy can be obtained by giving the infalling particle a high energy $E_0>1$. In the following example, the pair (L_0,E_0) should be chosen above the curve of unstable circular orbits with negative angular momenta (see Fig. 5).

(1) It turns out that it is possible for a particle with an angular momentum L_0 to fall inward toward $(\rho_C,0)$, at which point the corresponding circular orbit has angular momentum $L_-(\rho_C)=L_0$. If the infalling particle remains within the plane of the disk, it suffices to check that (2) holds at $(\rho_C,0)$. In the diagram (E,h), the graph of the function

$$h(E)=\frac{1}{2}\left(1-\frac{1}{\rho_C^2}\left[L_0^2 g_{tt}(\rho_C,0)+2L_0 E g_{\varphi t}(\rho_C,0)+E^2 g_{\varphi\varphi}(\rho_C,0)\right]\right)$$

shows a parabola with negative curvature (since $g_{\varphi\varphi}>0$). Furthermore, $h[E_-(\rho_C)]=0$ since this just represents the first of the conditions (3) for the circular orbit at ρ_C with negative angular momentum. Another conclusion is

$$\frac{dh}{dE}[E_-(\rho_C)]=-\frac{1}{\rho_C^2}\left[L_0 g_{\varphi t}(\rho_C,0)+E_-(\rho_C) g_{\varphi\varphi}(\rho_C,0)\right]=-\dot{t}_C<0,$$

where $\dot{t}_C$ denotes the fourth component of the four velocity of the circular orbit at ρ_C. Thus, h is negative for $E>E_-(\rho_C)$ and hence in particular for $E=E_0$. The infalling particle reaches the point $(\rho_C,0)$.

(2) At the point $(\rho_C,0)$ the particle splits. One of the created particles follows the circular path at ρ_C with negative angular momentum. Hence, it possesses the energy $E_1=E_-(\rho_K)$. The angular momentum of the escaping particle vanishes, whereas its energy $E_2=E_0-E_1$ is greater than E_0 if $E_-(\rho_C)$ is negative. Again, it can be shown that the escaping particle indeed reaches the point $(\rho_C,0)$.

If one goes along the curve of unstable circular orbits (Fig. 5) to higher and higher energies, the corresponding $E_-(\rho_C)$ will be of higher and higher magnitude. Hence, an arbitrary high amount of energy can be obtained if the infalling particle carries a high energy (and a corresponding angular momentum L_0). An example of the described Penrose effect is displayed in Fig. 8.

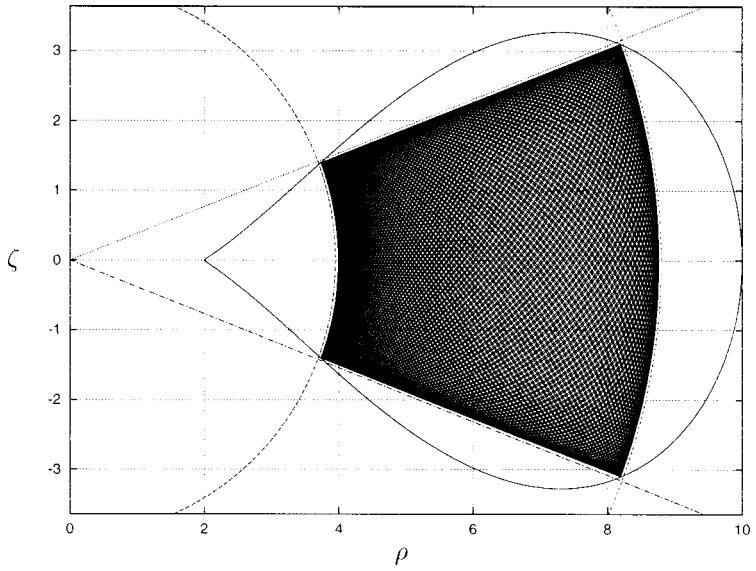

FIG. 9. Example of a geodesic motion in the (ρ,ζ) space with the values $\mu=1$, $L=-1.32$, $E=0.8$, $\rho_1=2$, $\rho_2=10$.

IV. HAMILTONIAN MECHANICS FOR THE GEODESICS

In this section the dynamical properties of bounded geodesics in phase space are investigated. Section IV A treats integrable motions. The regions in phase space occupied by the trajectories are discussed. Furthermore, a class of integrable Hamiltonians—the so-called Liouville class (see, e.g., Ref. 9)—is introduced. In Sec. IV B, this class will turn out to be relevant for the discussion of the nearly integrable geodesics and their properties. Finally, Sec. IV C treats the remaining geodesics which show highly stochastic behavior.

A. Integrable Hamiltonian systems

A famous theorem by Liouville states that in phase space, the bounded trajectories of an integrable Hamiltonian run on geometrical objects diffeomorphic to tori (for a proof see, e.g., Ref. 10). By means of a canonical transformation, it is possible to introduce angle and action variables (ϕ_j, I_j) in which the Hamiltonian merely depends on the action variables I_j. The corresponding Hamiltonian equations

$$\frac{dI_i}{d\tau}=-\frac{\partial \mathscr{H}(I_j)}{\partial \phi_i}=0, \quad \frac{d\phi_i}{d\tau}=\frac{\partial \mathscr{H}(I_j)}{\partial I_i}=\text{const}$$

are easily integrated; one gets $I_j=\text{const}$ and $\phi_j=\omega_j\tau+\phi_{j0}$, where ω_j and ϕ_{j0} are constants.

For an integrable Hamiltonian with two degrees of freedom, one can describe the situation as follows. In the four-dimensional phase space, the action variables $I_j (j=1,2)$ determine a set of surfaces diffeomorphic to two-dimensional tori. Each bounded motion of the considered integrable Hamiltonian runs on one of these surfaces. The angle variables yield a coordinate net on this surface, and the motion within this net proceeds linearly in time. If the ratio ω_1/ω_2 is chosen to be rational, the motion is periodic on the surface; for a ratio $\omega_1/\omega_2=m/n$ $(m,n\in\mathbb{N}$; relatively prime), the path returns to its initial point after a time period of $\tau=2\pi m/\omega_1$. Since the rational numbers are dense in the set of real numbers, the surfaces $I_j=\text{const}$ on which the motion is periodic form a dense subset in the set of all surfaces $I_j=\text{const}$. For the nonperiodic motions with an irrational ratio of the frequencies ω_1 and ω_2, the trajectory fills uniquely the whole surface.

Trajectories in phase space are studied by means of the so-called Poincaré surfaces of section. One chooses a two-dimensional surface in the phase space and labels its two sides (say left and right). Then, the set of crossing points of the trajectory through this surface is investigated. Only intersections are considered for which the trajectory runs through the surface in a particular sense (say from left to right). For integrable Hamiltonians, one gets a closed curve if the ratio of the frequencies is irrational. Otherwise, the Poincaré surfaces of section contain a finite number of

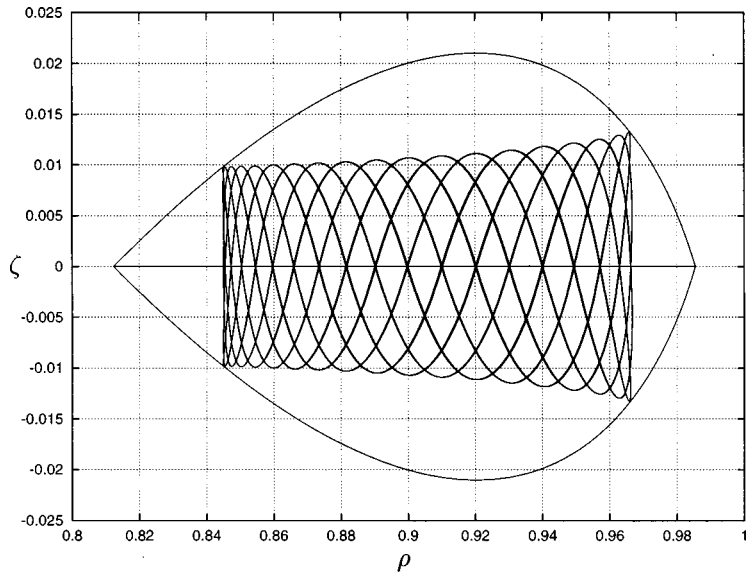

FIG. 10. Example of a geodesic motion in the (ρ,ζ) space with the values $\mu=3$, $L=2.78$, $E=0.77$, $\rho_1=0.81$, $\rho_2=0.986$.

intersection points. For continuously chosen initial conditions of the action variables I_j, the resulting picture consists of closed curves lying inside one another. Lying densely between them, are the finitely many intersection points corresponding to periodic motions.

An important family of integrable Hamiltonian is the so-called Liouville class. In Sec. IV B it will turn out to be the class to which the Hamiltonians for the geodesics are close.

(1) A conformal coordinate transformation $\rho'=\rho'(\rho,\zeta)$ and $\zeta'=\zeta'(\rho,\zeta)$ is defined such that the complex function $z'=z'(\rho,\zeta)=\rho'(\rho,\zeta)+i\zeta'(\rho,\zeta)$ can be expressed only in terms of the variable $z=\rho+i\zeta$, i.e., $z'=z'(z)$. In these coordinates, Hamiltonian systems of the form (1), i.e.,

$$\mathscr{H}=\tfrac{1}{2}e^{\alpha(\rho,\zeta)}(p_\rho^2+p_\zeta^2)+h(\rho,\zeta;L,E), \tag{5}$$

assume the form

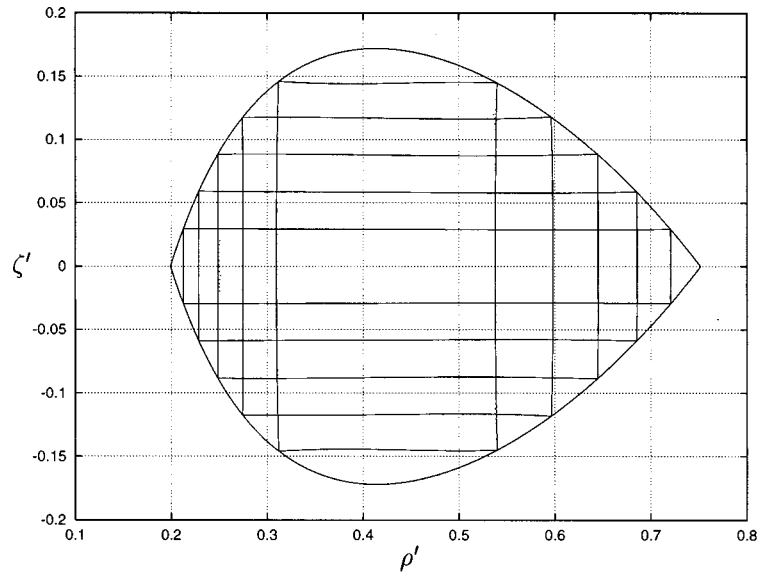

FIG. 11. Boundaries of regions that are filled by Newtonian geodesics in the conformal coordinates (ρ',ζ') introduced by $z'=10z/(10+z^2)$ (the values $\rho_1=0.2$, $\rho_2=0.75$ have been taken).

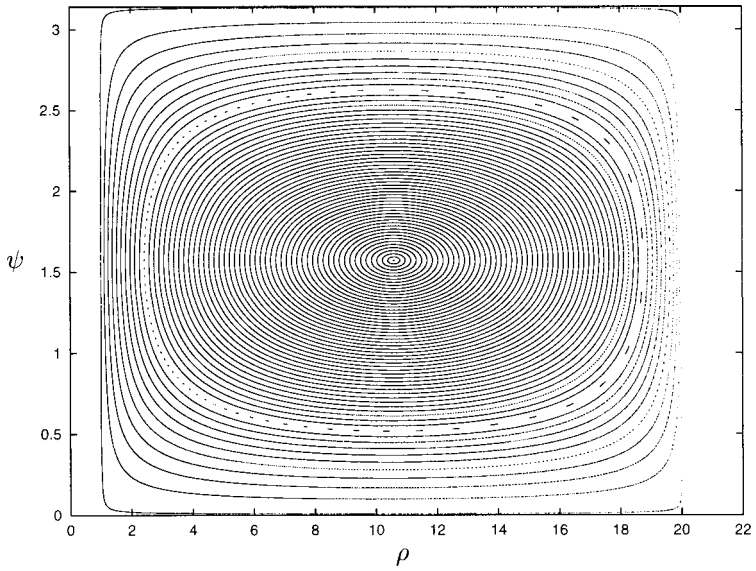

FIG. 12. Poincaré section of surface with $\rho_1=1.0001$, $\rho_2=20$ (Maclaurin disk).

$$\mathscr{H}=\tfrac{1}{2}e^{\alpha'(\rho',\zeta')}(p_{\rho'}^2+p_{\zeta'}^2)+h'(\rho',\zeta';L,E)$$

with

$$e^{\alpha'}=e^{\alpha}\left|\frac{dz'}{dz}\right|^2, \quad h'(\rho',\zeta';L,E)=h[\rho(\rho',\zeta'),\zeta(\rho',\zeta');L,E].$$

(2) A Hamiltonian system of the form (5) turns out to be integrable if there are conformal coordinates $z'=z'(z)$ in which the functions α' and h' read

$$e^{\alpha'(\rho',\zeta')}=\frac{1}{R_1(\rho')+Z_1(\zeta')},$$

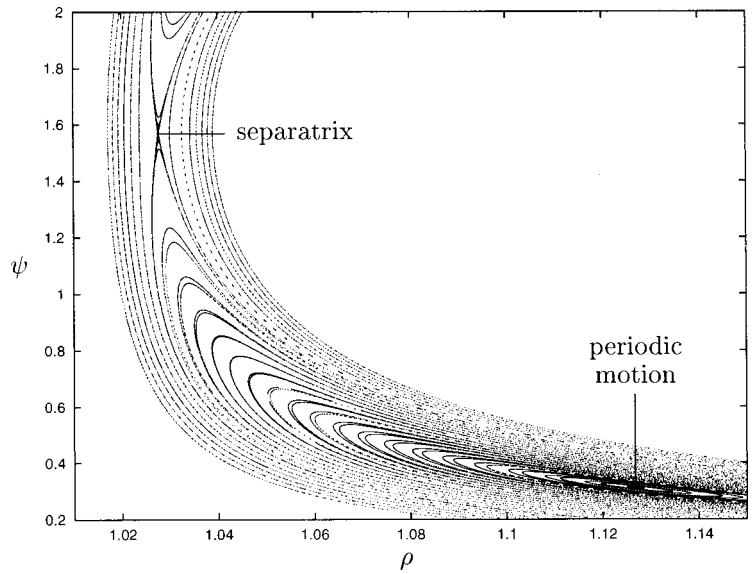

FIG. 13. Magnified extract from Fig. 12.

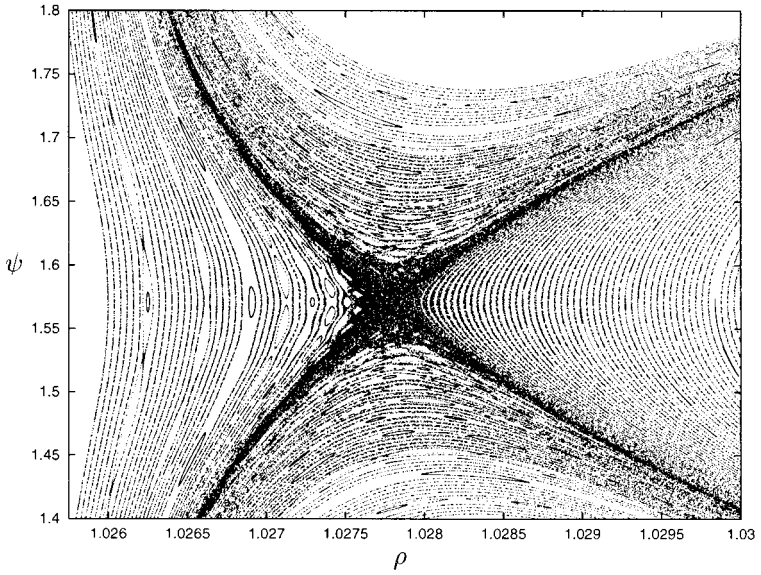

FIG. 14. Still more strongly magnified extract from Fig. 12.

$$h'(\rho',\zeta')=\frac{1}{2}\,e^{\alpha'(\rho',\zeta')}[R_2(\rho')+Z_2(\zeta')]=\frac{1}{2}\cdot\frac{R_2(\rho')+Z_2(\zeta')}{R_1(\rho')+Z_1(\zeta')},$$

where the functions R_i only depend on ρ' and the functions Z_i only on ζ'. Hamiltonians possessing this property belong to the Liouville class of integrable systems. From their first integrals, one concludes

$$\frac{\dot{\rho}'^2}{\dot{\zeta}'^2}=\frac{\nu+2\lambda R_1-R_2}{-\nu+2\lambda Z_1-Z_2}=\frac{R_3(\rho';\lambda,\nu)}{Z_3(\zeta';\lambda,\nu)}.$$

If the constants of integration, λ and ν, are fixed by the conditions $R_3(\rho_1';\lambda,\nu)=0=R_3(\rho_2';\lambda,\nu)$, then $\dot{\rho}'$ vanishes whenever the coordinate ρ' reaches the values ρ_1' or ρ_2'. Simi-

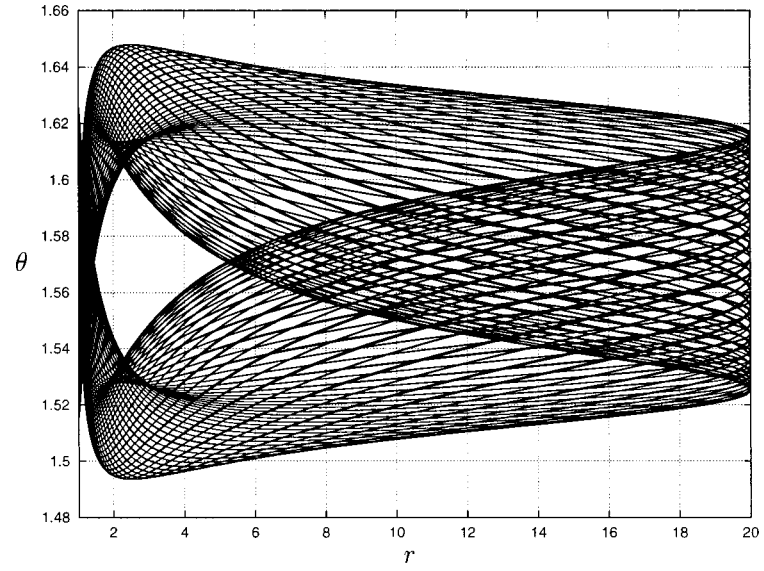

FIG. 15. Trajectory whose intersection points on the Poincaré surface of section fall into the regions of islands displayed in Fig. 13. The curve is presented in spherical polar coordinates ($\rho=r\sin\theta$; $\zeta=r\cos\theta$).

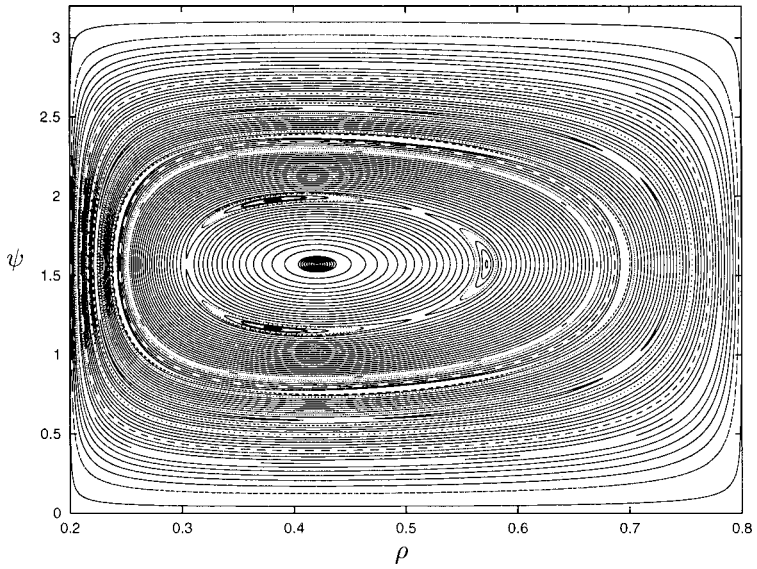

FIG. 16. Poincaré section of surface with $\rho_1=0.2$, $\rho_2=0.8$ (Maclaurin disk).

larly, $\dot{\zeta}'$ vanishes whenever the coordinate ζ' assumes the value of a zero of the function $Z_3(\zeta';\lambda,\nu)$, of which there are at least two for bounded motions. Thus, any bounded nonperiodic motion will gradually fill a region which is spanned by the coordinate axes $\rho'=\text{const}$ and $\zeta'=\text{const}$.

It can be shown that the geodesics within the Kerr metric (the integrability of which was proved by Carter[10]) belong to this class. One gets another important special case by introducing the conformal coordinates $z'=z'(z)=\ln z$, which are closely connected with spherical polar coordinates. Thus, there is a class of integrable Hamiltonians whose (nonperiodic) trajectories in the (ρ,ζ) space densely fill circular segments.

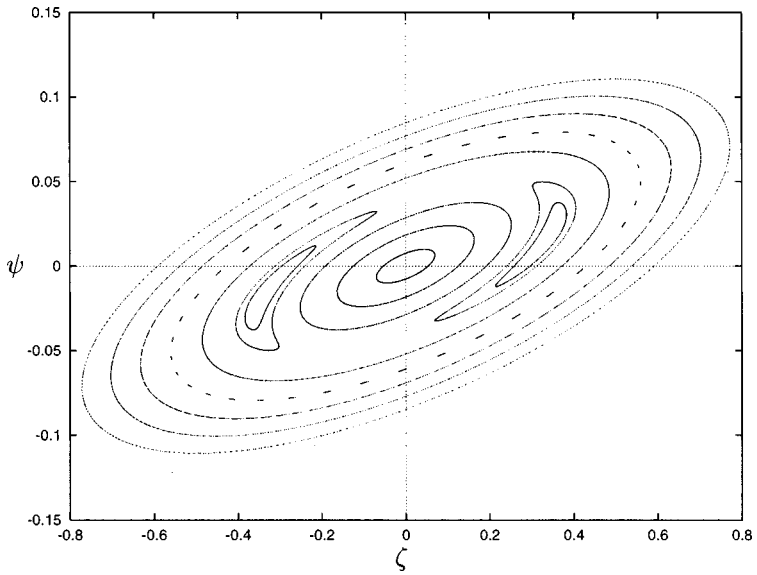

FIG. 17. Poincaré section of surface with $\mu=3.5$, $\rho_1=1.01$, $\rho_2=20$ (relativistic disk). The plane $\rho=\frac{1}{2}(\rho_1+\rho_2)$ and the crossing direction $\dot{\rho}>0$ have been taken.

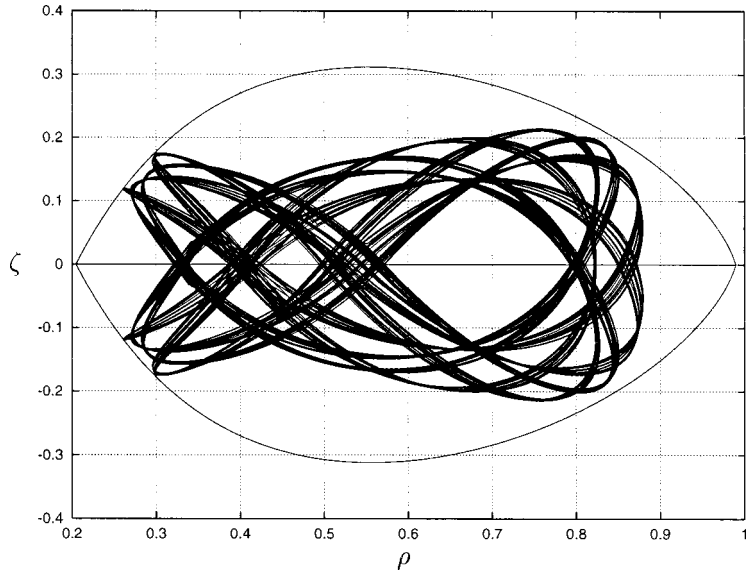

FIG. 18. Example of clearly irregular relativistic geodesic ($\mu=1$, $\rho_1=0.205$, $\rho_2=0.99$).

B. Nearly integrable Hamiltonian systems

Figures 9 and 10 show examples of bounded geodesic motions. In the (ρ,ζ) space, the paths remain within a certain region determined by the formula (2). In Fig. 9, both intersection points (with ρ coordinates ρ_1 and ρ_2) of this region with the disk of the plane are outside the disk, whereas in Fig. 10 both of them are placed inside.

One notices a high regularity of the resulting geodesics. From Fig. 9, one gets the impression that the corresponding Hamiltonian possesses, in spherical polar coordinates, the separation property discussed in Sec. IV A. Also the geodesic shown in Fig. 10 seems to belong to an integrable system of the Liouville class. In Fig. 11, the boundaries of the regions that are gradually filled by the geodesics can be seen in conformal coordinates which are introduced by the transformation $z'=10z/(10+z^2)$.

However, these systems turned out to be clearly nonintegrable. But their deviations from

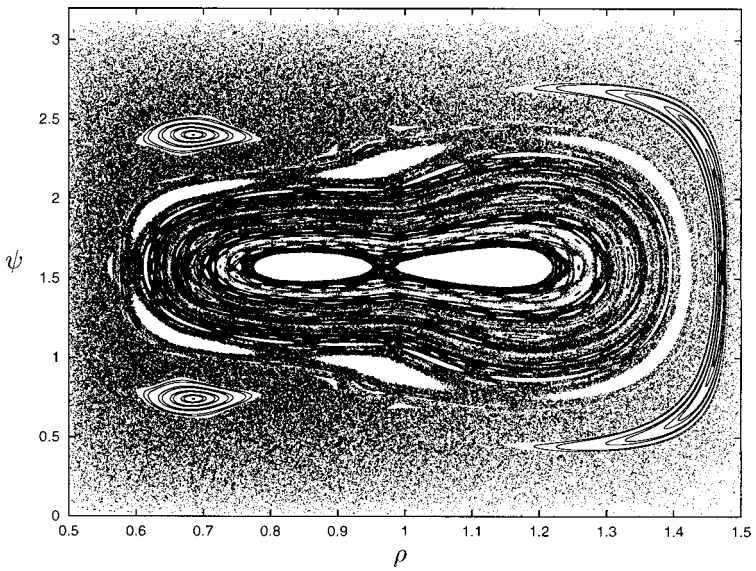

FIG. 19. Poincaré section of surface with $\rho_1=0.5$, $\rho_2=1.5$ (Maclaurin disk).

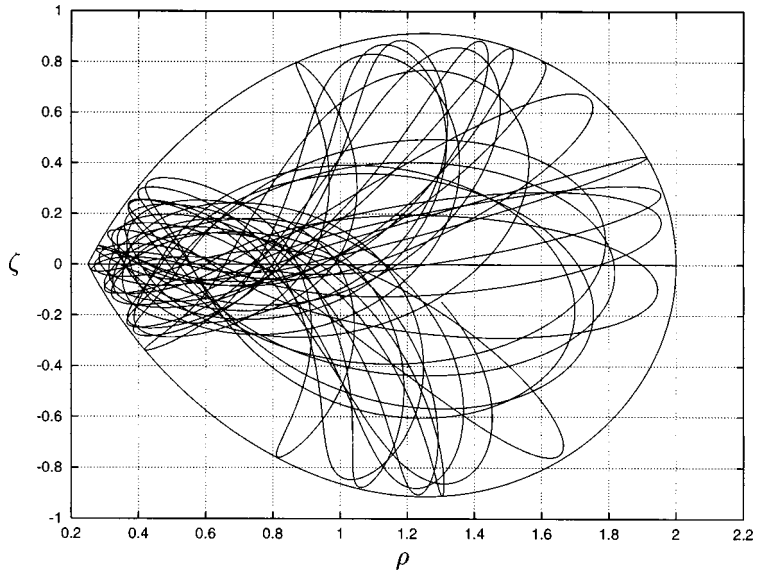

FIG. 20. Example of a geodesic motion in the (ρ,ζ) space with the values $\mu=1$, $L=-0.57$, $E=0.89$, $\rho_1=0.25$, $\rho_2=2$.

integrable systems of the Liouville class are so small that the so-called KAM (Kolmogorov, Arnold, Moser) theorem (see, e.g., Ref. 11) for nearly integrable systems applies.

According to this theorem, the qualitative characteristics of the trajectories of a weakly disturbed integrable Hamiltonian do not change drastically. Most of the curves are still regular, i.e., they are associated with first integrals of motion. Some of the trajectories still lie on tori which now are slightly deformed compared to the integrable case. However, the most regular motions occur on more complicated surfaces. Insight into the topological structure of these surfaces is given by the Poincaré sections of surface. The remaining geodesics show irregular behavior and are not associated with first integrals of motion.

The situation is illustrated by the Poincaré sections of surface displayed in Figs. 12–14. The trajectories are considered in the three-dimensional hypersurface $\mathscr{H}=0$. A coordinate net in this space is given by the coordinates ρ, ζ, and ψ where the angle ψ is defined by $\tan\psi=\dot{\zeta}/\dot{\rho}$. For the Poincaré sections of surface, the intersection plane $\zeta=0$ and the crossing direction $\dot{\zeta}>0$ have

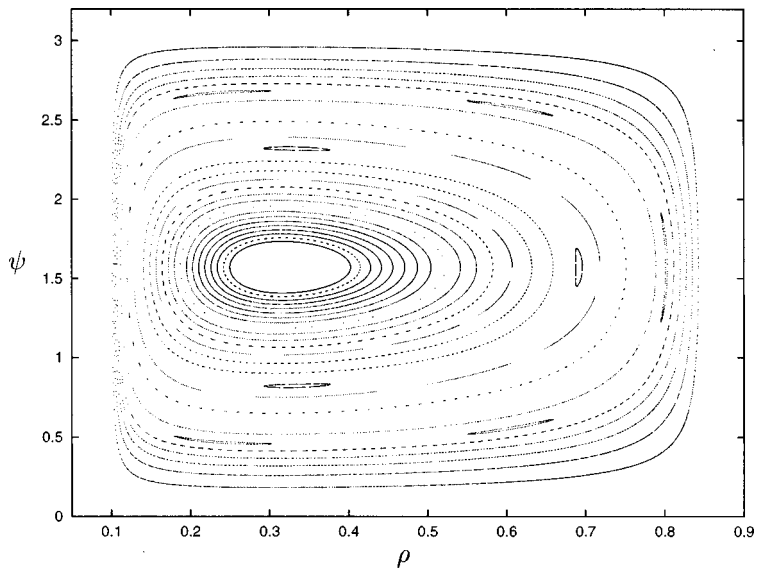

FIG. 21. Poincaré section of surface with $\rho_1=0.1$, $\rho_2=0.85$ (Maclaurin disk).

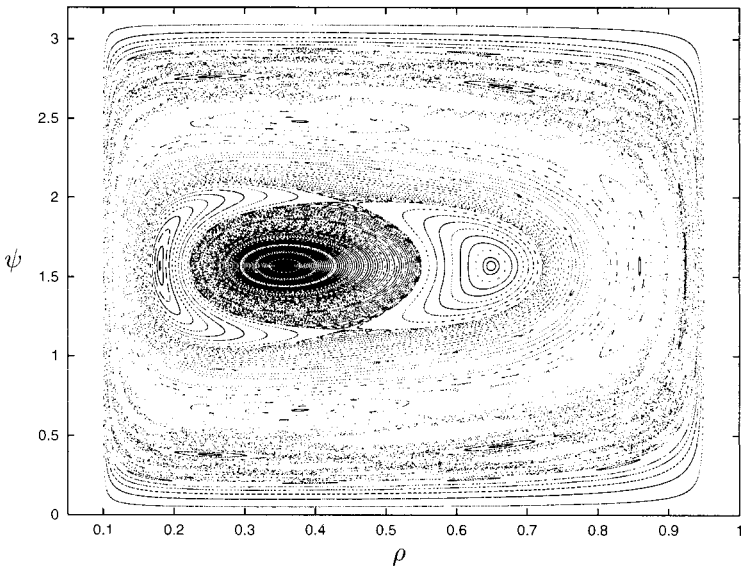

FIG. 22. Poincaré section of surface with $\rho_1 = 0.1$, $\rho_2 = 0.95$ (Maclaurin disk). The distances between the KAM tori have clearly enlarged. The irregular trajectories fill a considerable part of the phase space.

been taken. [The sections of surfaces were created by taking fixed values ρ_1 and ρ_2 and varying the initial conditions $(\rho(0),\zeta(0))$ of the trajectories continuously along the boundary of the region described by formula (2).]

At first glance, one sees as depicted in Fig. 12, what seems to simply be a series of curves lying inside one another, as described in Sec. IV A for integrable motions. But if one enlarges an extract, a more complicated structure becomes evident (Fig. 13). The periodic motions are encircled by islands which lie inside one another. Furthermore, there are so-called separatrices encircling different groups of these islands. In the vicinity of an apex between two of these groups of islands, one recognizes a still more complicated structure (Fig. 14). New groups of islands can be found, and at every new level of magnification, the same qualitative picture emerges. The separatrices represent irregular motions. However, each of the islands belongs to a regular one

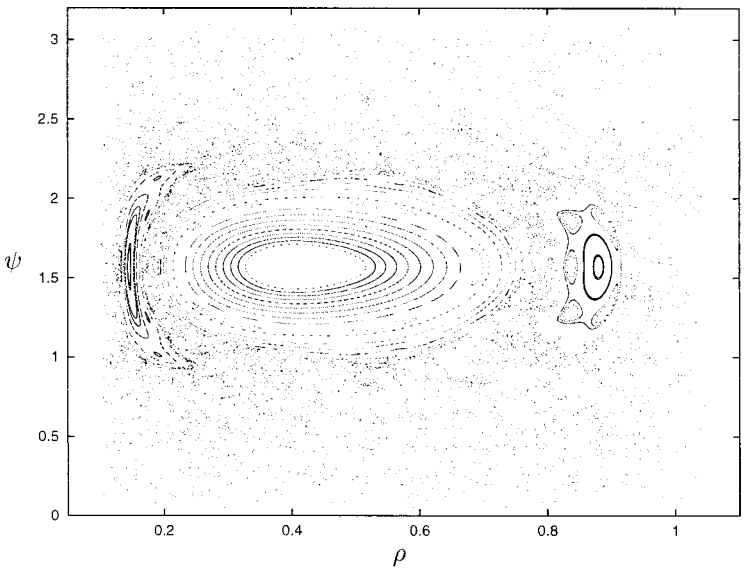

FIG. 23. Poincaré section of surface with $\rho_1 = 0.1$, $\rho_2 = 1.05$ (Maclaurin disk). The characteristical KAM tori have disappeared. Now, there are islands of regular motions within a region of globally stochastic motions.

(with a complicated topological structure of the surface on which the trajectory is trapped). An example for a such a geodesic motion is to be seen in Fig. 15.

Also the geodesics, for which the corresponding region of motion given by formula (2) intersects the plane of the disk at the ρ values $\rho_1<\rho_2<1$, prove to be nearly integrable. As to be seen in Fig. 16, they are not as close to integrable systems as those for the case $1<\rho_1<\rho_2$. But one gets the same qualitative pictures.

The qualitative properties discussed above can be found for the Maclaurin disk (i.e., the Newtonian limit) as well as for the relativistic disk. In general, the relativistic motions show a somewhat stronger deviation from integrable systems, but they still can be regarded as nearly integrable motions. A Poincaré section of surface for the relativistic disk can be seen in Fig. 17. A clearly irregular motion is displayed in Fig. 18.

From these investigations one concludes that the regions in the (ρ,ζ) space that are gradually filled by the nonperiodic geodesics are not spanned by the coordinate axis $\rho'=\text{const}$ and $\zeta'=\text{const}$ of a conformal coordinate system. Rather one finds that the trajectories are trapped by neighboring regions of this form. The distance between these neighboring regions is determined by the deviation of the geodesic in question from an integrable motion.

C. Global stochastic motions

As the departures from an integrable Hamiltonian grow, the distances between the regular curves in phase space become larger and larger. If the disturbance is large enough, then there are no longer any KAM tori, which previously encircled the irregular trajectories. In a global stochastic region, smaller subregions occur, containing groups of islands similar to those described in Sec. IV B. Again, these islands correspond to regular motions.

The remaining bounded geodesic motions, for which the boundary of the region described by formula (2) intersects the plane of the disk at the ρ coordinates $\rho_1<1<\rho_2$, show just this stochastic behavior (as can be seen in Figs. 19 and 20).

The transition from nearly integrable systems to the global stochastic ones is indicated in Figs. 21–23. Here, while keeping the value $\rho_1<1$ fixed, the coordinate ρ_2 is gradually enlarged, which eventually leads to the global stochastic picture in which the KAM tori have disappeared.

Global stochastic motions possess a rather unpredictable behavior. In general, the trajectories are not necessarily trapped into a subregion of the region described by (2) (as was the case for nearly integrable motions). However, if one restricts oneself to motions which lie in a region of islands, one has again nearly integrable motions with particular properties. (For a detailed introduction into the theory of regular and stochastic motions, see, e.g., Ref. 12.)

ACKNOWLEDGMENTS

My warmest thanks go to R. Meinel and G. Neugebauer for their hints and support.

[1] J. M. Bardeen, in *Black Holes*, edited by C. DeWitt and B. S. DeWitt (Gordon and Breach, New York, 1973), p. 219.
[2] B. Carter, Phys. Rev. **174**, 1559 (1970).
[3] J. M. Bardeen and R. V. Wagoner, Astrophys. J. **167**, 359 (1971).
[4] G. Neugebauer and R. Meinel, Phys. Rev. Lett. **75**, 3046 (1995).
[5] F. J. Ernst, Phys. Rev. **167**, 1175 (1968).
[6] D. Kramer and G. Neugebauer, Commun. Math. Phys. **7**, 173 (1968).
[7] R. Meinel and A. Kleinwächter, Einstein Studies (Birkhäuser) **6**, 339 (1995).
[8] G. Neugebauer, A. Kleinwächter, and R. Meinel, Helv. Phys. Acta **69**, 472 (1996).
[9] G. Contopoulos, in *Galactic Dynamics and N-Body Simulations* (Springer, Berlin, 1994), p. 50.
[10] V. I. Arnold, *Mathematical Methods of Classical Mechanics* (Springer, New York, 1978, 1989), p. 271.
[11] See Ref. 9, p. 405.
[12] A. J. Lichtenberg and M. A. Liebermann, *Regular and Stochastic Motion* (Springer, New York, 1983), pp. 158–178.